

A vector quantized masked autoencoder for audiovisual speech emotion recognition*

Samir Sadok^{a,*}, Simon Leglaive^a, Renaud Séguier^a

^aCentraleSupélec, IETR UMR CNRS 6164, France

Abstract

The limited availability of labeled data is a major challenge in audiovisual speech emotion recognition (SER). Self-supervised learning approaches have recently been proposed to mitigate the need for labeled data in various applications. This paper proposes the VQ-MAE-AV model, a vector quantized masked autoencoder (MAE) designed for audiovisual speech self-supervised representation learning and applied to SER. Unlike previous approaches, the proposed method employs a self-supervised paradigm based on discrete audio and visual speech representations learned by vector quantized variational autoencoders. A multimodal MAE with self- or cross-attention mechanisms is proposed to fuse the audio and visual speech modalities and to learn local and global representations of the audiovisual speech sequence, which are then used for an SER downstream task. Experimental results show that the proposed approach, which is pre-trained on the VoxCeleb2 database and fine-tuned on standard emotional audiovisual speech datasets, outperforms the state-of-the-art audiovisual SER methods. Extensive ablation experiments are also provided to assess the contribution of the different model components.

Keywords: Self-supervised learning, Masked autoencoder, Audiovisual speech processing, Emotion recognition

1. Introduction

Emotion recognition (El Ayadi et al., 2011) aims to automatically identify emotions from unimodal or multimodal data. With the increasing prevalence of audiovisual interfaces, there is a growing need for systems that can accurately recognize emotions from audiovisual speech data. The complementarity of the audio and visual modalities has been demonstrated in various tasks (Gan et al., 2020; Gao & Grauman, 2019; Zhao et al., 2019; Sadok et al., 2024), and using them together can lead to more effective emotion recognition systems. According to Mehrabian (2017), only a small proportion of feelings and emotions is conveyed through the words we use in oral communication. The majority of our feelings and emotions is conveyed through tone, voice, facial expressions, and body language. In recent years, advances in artificial intelligence technology and hardware acceleration have enabled a shift towards multimodal processing in the field of emotion recognition (Rama-chandram & Taylor, 2017; Tsai et al., 2019; Schoneveld et al., 2021). Supervised learning using large annotated datasets remains the dominating paradigm. However, collecting a substantial amount of emotionally labeled data can be expensive, time-consuming, and sometimes impractical. Most datasets for emotion recognition rely on actors to perform various emotions at specific intensities, which

requires a considerable amount of acquisition time and resources. In addition, in-the-wild datasets suffer from annotation issues, where annotators fail to reach a consensus, resulting in a significant amount of unusable data (Busso et al., 2008). Unsupervised and self-supervised learning (SSL) approaches are natural ways to address these issues and have been explored in recent studies (Bengio et al., 2006; Wang et al., 2021; Dib et al., 2023), (Chen & Rudnicky, 2023). SSL offers the advantage of high scalability, as the SSL task can be carried out on large amounts of unlabeled speech data (Liu et al., 2022; Zhang et al., 2022). These methods involve pre-training models with pretext tasks and then fine-tuning them on a smaller set of labeled data for the emotion recognition task (Gong et al., 2022a; Pepino et al., 2021; Jegorova et al., 2023).

In this paper, we introduce the VQ-MAE-AV model, a vector quantized (VQ) masked autoencoder (MAE) for audiovisual (AV) speech representation learning applied to audiovisual SER. The overall architecture of the model is illustrated in Fig. 1 and 2. To the best of our knowledge, this is the first multimodal SSL approach based on MAEs (He et al., 2022) that is proposed for audiovisual SER. Moreover, unlike existing multimodal MAEs proposed in other application contexts (Bachmann et al., 2022; Geng et al., 2022), the VQ-MAE-AV model operates on discrete latent representations of the modalities and introduces global tokens that are learned using contrastive learning to capture the overall sequence-wise information from each modality. The VQ-MAE-AV model is pre-trained on the VoxCeleb2 dataset (Chung et al., 2018) and fine-tuned on two standard emotional audiovisual speech datasets. The

*This paper was submitted to the Computer Vision and Image Understanding journal.

*Corresponding authors

Email address: samir.sadok@centralesupelec.fr (Samir Sadok)

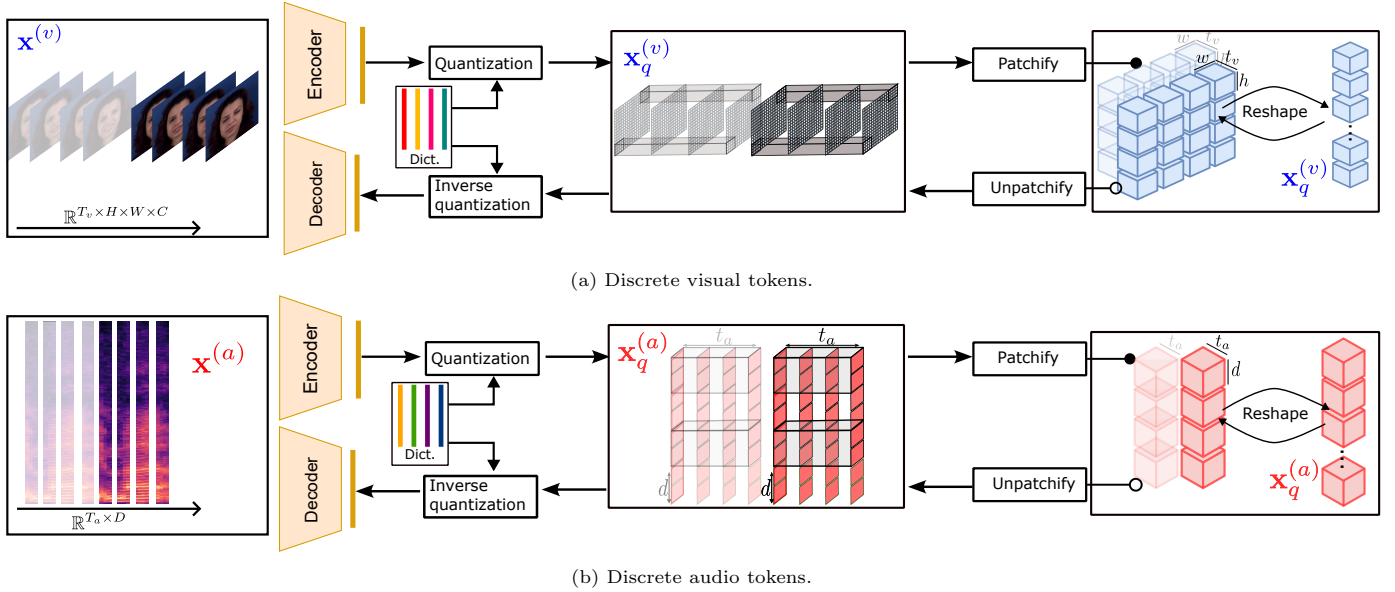


Figure 1: Discrete audio and visual tokens creation: (i) fully-convolutional VQ-VAEs are trained independently on the audio and visual modalities (see Section 3.1); (ii) discrete audio and visual tokens are built from the quantized representations provided by the frozen VQ-VAE encoders (see Section 3.2).

experimental results demonstrate that, across the two test datasets, the proposed VQ-MAE-AV model outperforms the state-of-the-art audiovisual SER methods. Extensive ablation experiments are also presented to study the impact of different model designs. The code and qualitative results are available at <https://samsad35.github.io/VQ-MAE-AV>.

2. Related work

Self-supervised learning approaches. SSL models can be broadly categorized into discriminative and generative approaches (Zhang et al., 2022). Discriminative SSL focuses on creating pairs or groups of data samples and formulating loss functions that enable the model to distinguish or group these samples, which can later benefit downstream tasks (Chen et al., 2020b,a). Pretext tasks can consist of solving jigsaw puzzles (Noroozi & Favaro, 2016) or predicting image rotations (Gidaris et al., 2018) for example. Contrastive learning has emerged as the predominant paradigm in discriminative SSL (Alayrac et al., 2020; Akbari et al., 2021). In contrast, generative SSL involves generating or reconstructing segments of unlabeled and potentially corrupted data using an autoencoder model (He et al., 2022; Bao et al., 2021; Xie et al., 2022). The latent representation produced by the encoder can subsequently be used for downstream tasks.

Masked autoencoder. The present paper focuses on the MAE, an SSL generative model that uses an asymmetric encoder-decoder architecture with input masking (He et al., 2022). The MAE approach is inspired by masked language modeling (Devlin et al., 2019) and has been successfully applied to image modeling thanks to the development of

Vision Transformers (ViT) (Dosovitskiy et al., 2020). The MAE has recently been adapted for audio using a 2D time-frequency representation (Gong et al., 2022a; Baade et al., 2022; Huang et al., 2022). In the MAE paradigm, the input is divided into non-overlapping patches, each represented by a token embedding. A proportion of tokens are masked, typically 75% for image/audio modeling and 15% for text modeling, and only the visible tokens are fed to the encoder. The encoder outputs are used to reconstruct the masked tokens through a lightweight decoder. To successfully reconstruct the masked tokens, the encoder must generate a semantic representation, which can then be effectively transferred to downstream tasks (He et al., 2022). It was recently shown that combining the task of reconstructing masked tokens with contrastive learning can improve the representation learned by an MAE (Huang et al., 2023; Gong et al., 2022a).

Extensions of MAE for sequential and multimodal representation learning. A recent extension of the MAE was presented in (Feichtenhofer et al., 2022; Tong et al., 2022) for modeling image sequences, called Video-MAE. It uses the same architecture as the vanilla MAE (He et al., 2022) but incorporates a masking process from video ViT (ViViT) (Arnab et al., 2021). Since videos often contain redundant information, particularly in scenes with no motion, the authors propose a cubic masking approach along the temporal axis, combined with a high masking ratio of 90%. Other works have extended the MAE to handle multimodal data (Bachmann et al., 2022; Geng et al., 2022; Gong et al., 2022b). MultiMAE (Bachmann et al., 2022) encodes a small random subset of visible tokens from multiple modalities (RGB, depth, and semantic images) and is trained to reconstruct the missing ones. M3AE (Geng et al., 2022) is a unified

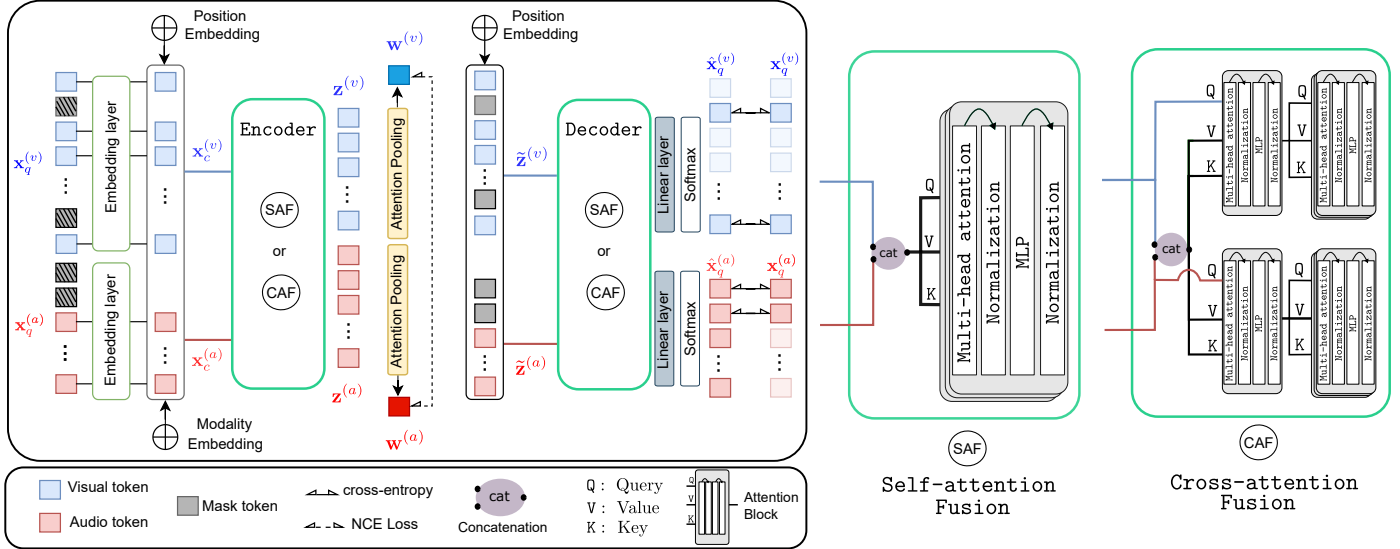


Figure 2: VQ-MAE-AV model structure. See the first paragraph of Section 3 for a complete description of the pipeline.

MAE architecture for two input modalities (image and text). The main difference in architecture between M3AE and MultiMAE lies in the architecture of the decoder. The MultiMAE approach introduces individual decoders for each modality, enhancing their fusion by incorporating a cross-attention layer at the outset of each decoder. On the other hand, the M3AE approach uses a single decoder that takes the concatenated tokens from all modalities as input.

Adaptation and improvement of the MAE. In the literature, MAEs are typically trained using the $L1$ or $L2$ losses, which can negatively affect the reconstruction quality of the masked tokens, resulting, for instance, in blurred or noisy images or sounds. It has been shown that improving the quality of MAE reconstructions can be beneficial in terms of downstream task performance (He et al., 2022). Several approaches have been proposed in that sense, which include adding a perceptual loss (Dong et al., 2021) or using discrete representations obtained from VQ generative adversarial networks (VQ-GANs) (Esser et al., 2021) or variational autoencoders (VQ-VAEs) (Van Den Oord et al., 2017) to train the MAE (Li et al., 2023; Sadok et al., 2023). These works only considered an unimodal setting, while the present paper proposes a multimodal MAE for audiovisual speech representation learning. Recently, a model called CAV-MAE (Gong et al., 2022b) was proposed combining MAEs and contrastive learning to learn a representation from audiovisual data. However, different from the proposed VQ-MAE-AV model, CAV-MAE processes raw audiovisual data instead of vector-quantized latent representations, it uses simple mean pooling strategies instead of attention pooling, and it is not applied to SER.

3. The VQ-MAE-AV model

This section presents the VQ-MAE-AV model. The overall approach is illustrated in Fig. 1 and 2 and it can

be summarized as follows:

- Fully-convolutional VQ-VAEs are trained independently on the audio and visual modalities (see Section 3.1);
- Discrete audio and visual tokens are built from the quantized representations provided by the frozen VQ-VAE encoders (see Section 3.2);
- A proportion of the discrete audio and visual tokens is masked out, using a coupled masking strategy between the two modalities (see Section 3.3);
- The visible audio and visual tokens are replaced with trainable continuous embedding vectors (see Section 3.4), which are fed to the VQ-MAE-AV encoder (see Sections 3.5.1 and 3.5.2, where we present two strategies based on attention mechanisms to fuse the modalities);
- Attention pooling is used to compute global sequence-wise tokens that are specific to each modality (see Section 3.5.3);
- The token-wise representation obtained from the encoder is combined with mask tokens and fed to the VQ-MAE-AV decoder, which tries to reconstruct the original discrete audio and visual tokens (see Section 3.5.4);
- The VQ-MAE-AV model is trained in a self-supervised manner to minimize (i) the cross-entropy loss between the reconstructed and original tokens and (ii) a contrastive loss between the audio and visual global tokens (see Section 3.6);
- After self-supervised learning, the VQ-MAE-AV encoder and attention pooling layers are fine-tuned for supervised audiovisual SER (see Section 3.7).

This section will present each above-listed aspect of the model in more detail.

3.1. Vector quantized variational autoencoder

The proposed multimodal self-supervised approach uses the discrete latent representation of two pre-trained and frozen VQ-VAEs (Van Den Oord et al., 2017). Specifically, as illustrated in Fig. 1, we use the VQ-VAE-audio and VQ-VAE-visual encoders to obtain compressed and quantized representations of the input speech power spectrogram $\mathbf{x}^{(a)} \in \mathbb{R}^{T_a \times D}$ where T_a and D correspond to the time and frequency dimensions, and of the input image sequence $\mathbf{x}^{(v)} \in \mathbb{R}^{T_v \times H \times W \times C}$ where T_v , H , W and C correspond to the time, height, width, and channel dimensions. The audio and visual quantized representations are denoted by $\mathbf{x}_q^{(a)} \in \mathbb{Z}^{T_a \times D'}$ and $\mathbf{x}_q^{(v)} \in \mathbb{Z}^{T_v \times H' \times W'}$, respectively. Each entry of $\mathbf{x}_q^{(a)}$ and $\mathbf{x}_q^{(v)}$ corresponds to the index of a vector in the VQ-VAE codebooks. Notably, $\mathbf{x}_q^{(a)}$ retains the time-frequency structure of the original spectrogram, while $\mathbf{x}_q^{(v)}$ retains the spatio-temporal structure of the original sequence images. This is because the VQ-VAE-audio and VQ-VAE-visual models are designed to be fully convolutional on the frequency and spatial axes, respectively, and they process the frames within a sequence independently. Therefore, compression occurs along the frequency axis ($D' \ll D$) for $\mathbf{x}_q^{(a)}$ and along the x and y-axes of the image ($H' \ll H$, $W' \ll W$) for $\mathbf{x}_q^{(v)}$. As shown in Fig. 2 and discussed in the following subsections, the proposed MAE-based self-supervised learning approach operates on these discrete and compressed representations before audiovisual speech reconstruction using the VQ-VAE decoders.

The training procedure of the VQ-VAEs follows the original approach presented in Van Den Oord et al. (2017). In particular, the VQ-VAE loss functions involve a reconstruction term between the original and reconstructed data, which corresponds to the mean squared error for the visual modality and to the Itakura-Saito divergence for the audio modality (Févotte et al., 2009). More details are provided in Section 4.1.2.

3.2. Discrete audio and visual tokens

As shown in Fig. 1, the audio and visual quantized representations $\mathbf{x}_q^{(a)} \in \mathbb{Z}^{T_a \times D'}$ and $\mathbf{x}_q^{(v)} \in \mathbb{Z}^{T_v \times H' \times W'}$ from the output of the VQ-VAE encoders are divided into non-overlapping patches to build discrete tokens $\mathbf{x}_q^{(a)} \in \mathbb{Z}^{(n_{t_a} \cdot t_a) \times (n_d \cdot d)}$ and $\mathbf{x}_q^{(v)} \in \mathbb{Z}^{(n_{t_v} \cdot t_v) \times (n_h \cdot h) \times (n_w \cdot w)}$, where $T_a = n_{t_a} \cdot t_a$, $D' = n_d \cdot d$, $T_v = n_{t_v} \cdot t_v$, $H' = n_h \cdot h$, and $W' = n_w \cdot w$. These representations are reshaped to $\mathbf{x}_q^{(a)} \in \mathbb{Z}^{(n_{t_a} \cdot n_d) \times (t_a \cdot d)}$ and $\mathbf{x}_q^{(v)} \in \mathbb{Z}^{(n_{t_v} \cdot n_h \cdot n_w) \times (t_v \cdot h \cdot w)}$, which are seen as sequences of $n_{t_a} \cdot n_d$ and $n_{t_v} \cdot n_h \cdot n_w$ tokens of dimension $t_a \cdot d$ and $t_v \cdot h \cdot w$, respectively.

The use of discrete audio and visual tokens in VQ-MAE-AV has several motivations. Firstly, by dividing the audiovisual data into spatio-spectro-temporal patches, the method could learn to relate audio tokens to visual tokens.

For example, the audio tokens are expected to correlate strongly with the visual tokens corresponding to the mouth area (Arel et al., 2016; Sadok et al., 2024). The proposed method can potentially learn a representation that captures shared and distinctive information between the two modalities by exploiting their complementarity. Additionally, the use of discrete tokens can reduce the computational cost of the method as it involves working with a reduced representation of the data, which allows us to increase the number of tokens (i.e., manipulate longer audiovisual speech sequences) without exploding in the number of trainable parameters compared to the multimodal MAE in the literature (Bachmann et al., 2022).

3.3. Masking

We apply masking to the audio and visual sequences of tokens. The MAE aims to reconstruct the masked tokens from the visible tokens to learn a semantic representation of the data. The masking strategy impacts the performance of downstream tasks. In the original MAE, the masked tokens are randomly drawn with a target ratio of the entire set of tokens, typically 75%. In multimodal scenarios, the basic strategy would be to do the same for each modality, but it has been shown that it is more interesting to implement a coupled masking strategy between the modalities (Bachmann et al., 2022). This involves randomly drawing a masking proportion $p_a \in [0, 1]$ for the audio modality and $p_v \in [0, 1]$ for the visual modality such that $p_a + p_v = 1$. To do this, a Dirichlet distribution is used: $(p_a, p_v) \sim \text{Dir}(\alpha_a, \alpha_v)$ where $\alpha_a, \alpha_v > 0$ are the concentration parameters of the distribution. When $\alpha_a = \alpha_v = 1$, the distribution is uniform overall points in its support (the 1-simplex), and $\alpha_a \gg \alpha_b$ results in a sampling behavior where most of the tokens are taken from the audio modality, and vice versa. These parameters can be used to reduce the dominance of one modality over the other. This strategy allows the reconstruction of missing information from one modality by relying on another. Therefore, the model will leverage the less masked modality for the reconstruction of the more masked one. For this paper, we set $\alpha_a = \alpha_v = 1$.

3.4. Continuous embedding vectors

The discrete tokens correspond to the indices obtained through the quantization step of the pretrained VQ-VAE encoder. Before being input to the VQ-MAE-AV encoder, these discrete tokens are replaced with trainable continuous embedding vectors taken from an audio codebook in $\mathbb{R}^{k_a \times e_a}$ and from a visual codebook in $\mathbb{R}^{k_v \times e_v}$, where $k_{a/v}$ is the number of codes in the codebook and $e_{a/v}$ is the dimension of each code. This is simply achieved by replacing the indices of a discrete token with the corresponding vectors of dimension $e_{a/v}$ in the codebook. After this embedding process, the sequences of discrete tokens $\mathbf{x}_q^{(a)} \in \mathbb{Z}^{(n_{t_a} \cdot n_d) \times (t_a \cdot d)}$ and $\mathbf{x}_q^{(v)} \in \mathbb{Z}^{(n_{t_v} \cdot n_h \cdot n_w) \times (t_v \cdot h \cdot w)}$ are transformed into sequences of continuous tokens $\mathbf{x}_c^{(a)} \in \mathbb{R}^{(n_{t_a} \cdot n_d) \times (t_a \cdot d \cdot e_a)}$ and $\mathbf{x}_c^{(v)} \in \mathbb{R}^{(n_{t_v} \cdot n_h \cdot n_w) \times (t_v \cdot h \cdot w \cdot e_v)}$.

3.5. VQ-MAE-AV encoder and decoder

3.5.1. Attention Block

The VQ-MAE-AV encoder and decoder are built with multi-head Attention blocks similar to those used in the Vision Transformer (ViT) (Dosovitskiy et al., 2020). Each block comprises a multi-head attention layer, normalization layers, and a Multi-layer Perceptron (MLP). These layers are interconnected with residual connections, as depicted in Fig. 2, and they will be used to capture the inter and intra-relationships between audio and visual tokens. This attention block is inspired by the attention layer in the original transformer (Vaswani et al., 2017). To simplify the reading afterward, we denote the attention block by $\text{Attention}(Q, V, K)$, where Q, V, K are the query, value, and key, respectively. The self-attention mechanism uses the same input vector for the query, key, and value vectors. In the case of cross-attention, the query and key are different to enable attention across multiple modalities or inputs.

3.5.2. Encoders

We propose two fusion strategies of the audio and visual speech data, resulting in two architectures for the VQ-MAE-AV encoder. The first fusion strategy is called *self-attention fusion* (SAF). As represented in Fig. 2, this fusion consists of a concatenation of token sequences for the two modalities, followed by L self-attention blocks. This concatenation operates on the first dimension of the variables, i.e., we obtain a sequence of $(n_{t_a} \cdot n_d) + (n_{t_v} \cdot n_h \cdot n_w)$ tokens after concatenation.

The second fusion strategy is called *cross-attention fusion* (CAF). As shown in Fig. 2, the sequences of audio and visual tokens are used separately as the queries of two separate attention blocks, which share the same keys and values corresponding to the concatenation of the modalities. These two cross-attention blocks are then followed by a stack of L self-attention blocks.

For both fusion strategies, the encoder outputs one sequence of tokens for each modality, denoted by $\mathbf{z}^{(a)}$ and $\mathbf{z}^{(v)}$.

3.5.3. Global tokens

In addition to the token-wise representations $\mathbf{z}^{(a)}$ and $\mathbf{z}^{(v)}$, we learn two sequence-wise global tokens, denoted by $\mathbf{w}^{(a)} \in \mathbb{R}^{1 \times (t_a \cdot d \cdot e_a)}$ and $\mathbf{w}^{(v)} \in \mathbb{R}^{1 \times (t_v \cdot h \cdot w \cdot e_v)}$, which can be thought of as similar to [CLS] tokens (He et al., 2022). These global modality-specific tokens are introduced to aggregate the spectro-temporal and spatio-temporal information in the two modalities, which can be useful for downstream tasks involving predictions at the sequence level, such as audiovisual SER. The global tokens are computed with attention pooling as follows:

$$\mathbf{w}^{(a)} = \text{Attention}(Q_{(a)}, V_{(a)}, K_{(a)}); \quad (1)$$

$$\mathbf{w}^{(v)} = \text{Attention}(Q_{(v)}, V_{(v)}, K_{(v)}), \quad (2)$$

where $Q_{(a)} = \mathcal{Z}^{(a)} \in \mathbb{R}^{1 \times (t_a \cdot d \cdot e_a)}$ and $Q_{(v)} = \mathcal{Z}^{(v)} \in \mathbb{R}^{1 \times (t_v \cdot h \cdot w \cdot e_v)}$ represent respectively trainable audio and visual tokens, as proposed in Touvron et al. (2021), $V_{(a)} = K_{(a)} = \mathbf{z}^{(a)}$, and $V_{(v)} = K_{(v)} = \mathbf{z}^{(v)}$.

3.5.4. Decoders

The token-wise representation obtained from the encoder is combined with mask tokens and fed to the VQ-MAE-AV decoder along with additional position embeddings, as denoted by $\tilde{\mathbf{z}}^{(a)}$ and $\tilde{\mathbf{z}}^{(v)}$ and illustrated in Fig. 2. The mask tokens actually correspond to one single trainable vector as proposed in the original MAE (He et al., 2022). Similarly as for the encoder, the audio and visual inputs of the VQ-MAE-AV decoder can be fused using either self-attention fusion or cross-attention fusion.

The number of attention blocks L' in the decoder is chosen to be lower compared to that of the encoder ($L' < L$).

A linear layer is added at the end of the decoder, which maps to the size of the VQ-VAE codebooks. The output of this linear layer corresponds to the logits of the discrete tokens. After applying a *softmax* operation, we obtain reconstructions $\hat{\mathbf{x}}_q^{(a)}$ and $\hat{\mathbf{x}}_q^{(v)}$ of the indices $\mathbf{x}_q^{(a)}$ and $\mathbf{x}_q^{(v)}$ that were provided by the VQ-VAE-audio and VQ-VAE-visual encoders, respectively.

3.6. VQ-MAE-AV loss functions

3.6.1. Generative loss function

To train the VQ-MAE-AV model, we minimize the cross-entropy loss applied only to the masked discrete tokens:

$$\begin{aligned} \mathcal{L}_{rec} = & \text{cross-entropy} \left(\mathbf{x}_q^{(a)} \left(\Omega_{\mathcal{M}}^{(a)} \right), \hat{\mathbf{x}}_q^{(a)} \left(\Omega_{\mathcal{M}}^{(a)} \right) \right) \\ & + \text{cross-entropy} \left(\mathbf{x}_q^{(v)} \left(\Omega_{\mathcal{M}}^{(v)} \right), \hat{\mathbf{x}}_q^{(v)} \left(\Omega_{\mathcal{M}}^{(v)} \right) \right), \quad (3) \end{aligned}$$

where $\mathbf{x} \left(\Omega_{\mathcal{M}}^{(\cdot)} \right)$ denotes the set of masked tokens in \mathbf{x} . Another benefit of manipulating discrete representations for multimodal inputs is the homogeneity of the losses, which does not require balancing the losses between the two modalities.

3.6.2. Contrastive loss function

Building upon the approaches presented in Alayrac et al. (2020); Akbari et al. (2021), the global tokens are learned using noise contrastive estimation. This approach enhances the alignment of audiovisual speech pairs by grouping together embeddings that belong to the same time sequence and separating them from those that do not correspond to the same sequence. This approach involves minimizing the

loss function $\mathcal{L}_{NCE}(\mathbf{w}^{(a)}, \mathbf{w}^{(v)})$, which is defined by:

$$\mathcal{L}_{NCE}(\mathbf{u}, \mathbf{v}) = -\log \left(\frac{\exp(\mathbf{u}^\top \mathbf{v} / \tau)}{\exp(\mathbf{u}^\top \mathbf{v} / \tau) + \sum_{(\mathbf{u}', \mathbf{v}') \in \mathcal{N}} \exp(\mathbf{u}'^\top \mathbf{v}' / \tau)} \right). \quad (4)$$

To form positive pairs $(\mathbf{w}^{(a)}, \mathbf{w}^{(v)})$ for both audio and visual modalities, we select corresponding streams from the same temporal location in the video. Conversely, negative pairs $(\mathbf{w}'^{(a)}, \mathbf{w}'^{(v)})$ are formed by selecting *non*-corresponding streams drawn from a set \mathcal{N} of different temporal locations for each batch. The sensitivity of the NCE loss in distinguishing between positive and negative pairs is regulated by a temperature parameter $\tau \in \mathbb{R}$.

3.6.3. Final loss function

The final loss function corresponds to the sum of the generative loss function in equation (3) and of the contrastive loss function in equation (4).

3.7. Fine-tuning for audiovisual SER

After pre-training VQ-MAE-AV on token unmasking, the model is fine-tuned for audiovisual SER. We propose three different approaches for fine-tuning the model. The first two approaches rely on a pooling operation (of the encoder outputs $\mathbf{z}^{(a)}$ and $\mathbf{z}^{(v)}$) to extract the global audio and visual tokens, which is either a simple *mean pooling* or the *attention pooling* discussed in Section 3.5.3. The extracted tokens are then concatenated and passed through a single linear layer, followed by an *argmax* operation to classify the emotion. The third proposed approach, referred to as *Query2Emo* and inspired by (Liu et al., 2021), involves cross-attention between all audio and visual tokens (concatenation of $\mathbf{z}^{(a)}$, $\mathbf{z}^{(v)}$) as key and value, and the emotion classes represented by trainable embeddings as the query. Query2Emo has a single attention block for both the encoder and decoder. The extracted embeddings are then concatenated and passed through a single linear layer. We adopt the asymmetric loss (Ridnik et al., 2021) for all these approaches between the predicted emotion and the ground-truth emotion.

4. Experiments

This section presents our study’s experimental setup and results, as well as a discussion of their implications. We evaluate the effectiveness of the proposed approach for emotion recognition on two standard audiovisual speech databases and compare it with state-of-the-art methods. Additionally, we perform an ablation study to analyze the impact of various hyperparameters and architectures on the performance of our method.

We present qualitative audio and visual reconstruction results in Fig. 3a and Fig. 3b, respectively. The reconstructions are illustrated for two distinct masking ratios: 50%

and 80%. Additional qualitative results are available online (see the webpage address at the end of Section 1). Furthermore, we conducted a study to measure the reconstruction quality at different masking ratios of the audiovisual speech data. This analysis is detailed in Section 4.2 and demonstrates the effectiveness of leveraging multimodality to enhance reconstruction quality.

4.1. Experimental setup

4.1.1. Datasets and preprocessing

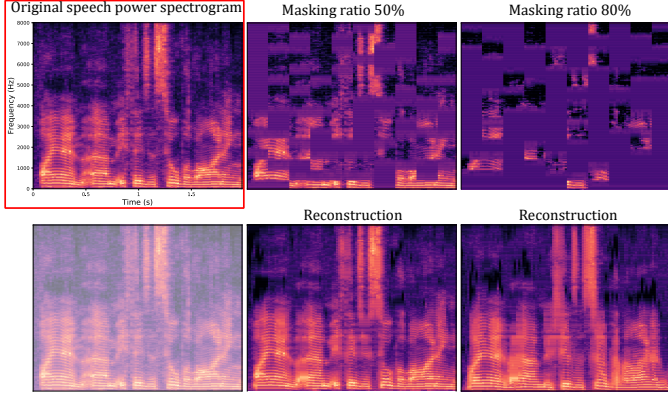
Dataset for self-supervised training. To pre-train VQ-MAE-AV, we use the VoxCeleb2 dataset (Chung et al., 2018), which offers a broad range of audiovisual speech data from open-source media, with each video featuring a single speaker. We restricted our dataset use to a subset of around 1000 hours of audiovisual speech, encompassing 2170 different speakers. The test set includes about 100 hours of audiovisual speech data with 117 different speakers.

Data pre-processing. The VQ-VAE-audio and VQ-VAE-visual models are trained on the VoxCeleb2 dataset. The former is trained on short-time Fourier transform (STFT) power spectrograms ($\mathbf{x}^{(a)}$), while the latter is trained on sequences of RGB images ($\mathbf{x}^{(v)}$) captured at 25 fps, cropped and resized to a resolution of 96×96 , and aligned using Face-Alignment (Bulat & Tzimiropoulos, 2017). To compute the STFT, a Hann window of 64 ms (1024 samples at 16 kHz) and a 68% overlap are used, resulting in a sample rate of 50 Hz, which is twice the sample rate of the visual modality. This leads to sequences of $D = 513$ Fourier coefficients.

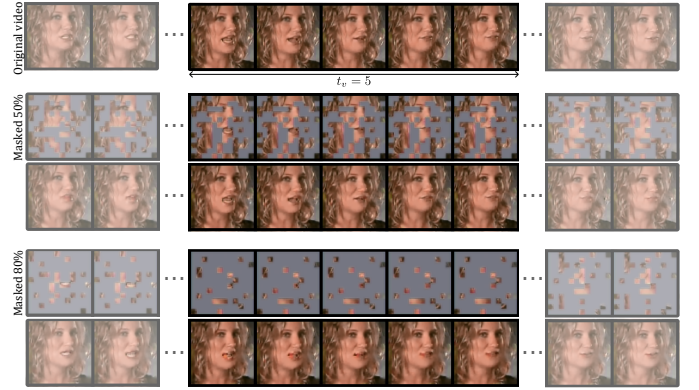
Emotional audiovisual speech databases. We fine-tune and evaluate the proposed approaches on two emotional audiovisual speech databases.

- **RAVDESS** (Livingstone & Russo, 2018): This English database consists of 1440 videos recorded by 24 professional actors and labeled with eight different emotions (neutral, calm, happy, sad, angry, fearful, disgust, surprised).
- **CREMA-D** (Cao et al., 2014): It is an English dataset of 7442 videos recorded by 91 actors. Actors spoke from a selection of 12 sentences. The sentences used one of six emotions (anger, disgust, fear, happy, neutral, and sad) with four different intensities (low, medium, high, and unspecified).

We selected these databases as they are commonly used for the emotion recognition task, and their raw data is accessible. We performed 6-fold and 10-fold cross-validation for the RAVDESS and CREMA-D datasets to ensure a fair comparison with previous works. The speaker identities are different in the fine-tuning and evaluation phases.

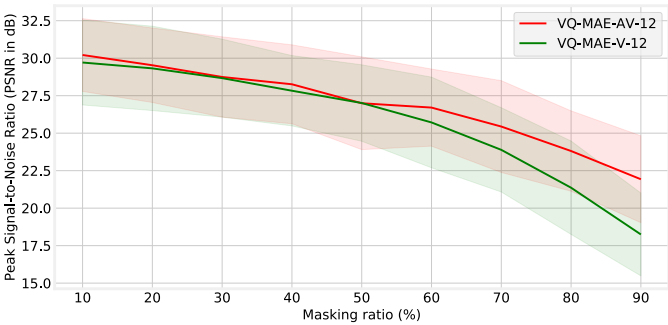


(a) Qualitative unmasking results for the audio modality. The spectrogram highlighted in the red box represents the original spectrogram. The two spectrograms on the top right represent the spectrograms masked at 50% and 80%, respectively. The reconstructions using VQ-MAE-AV can be seen directly below these masked spectrograms.

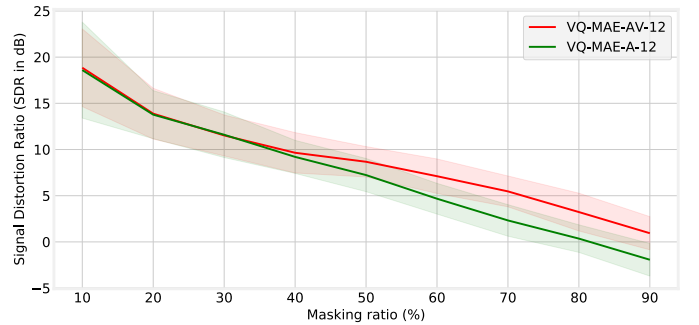


(b) Qualitative unmasking results for the visual modality. The first sequence shows the original video, followed by the next two sequences representing the masked video with a ratio of 50% and its reconstruction using VQ-MAE-AV. The last two sequences represent the masked video with a ratio of 80% and its reconstruction using VQ-MAE-AV.

Figure 3: Quantitative results of the audio reconstruction (a) and visual reconstruction (b) using the VQ-MAE-AV model.



(a) Peak Signal-to-Noise Ratio (PSNR in dB) on the y-axis as a function of masking ratio (%) on the x-axis.



(b) Signal-to-Distortion Ratio (SDR in dB) on the y-axis as a function of masking ratio (%) on the x-axis.

Figure 4: Quantitative results of the visual reconstruction (a) and audio reconstruction (b). The line represents the mean value across the test dataset, while the shaded area depicts the standard deviation.

4.1.2. Model architecture

VQ-VAE architectures. The VQ-VAE-audio (respectively VQ-VAE-visual) architecture is symmetrical concerning the encoder and the decoder, with three 1D (respectively 2D) convolution for the encoder or transposed convolution for the decoder layers and a residual convolution layer. The VQ-VAE models process each frame independently with no time dependency. For each speech power spectrogram frame of size $D = 513$, the VQ-VAE-audio encoder compresses it into a discrete latent vector (a column of $\mathbf{x}_q^{(a)}$) of size $D' = 64$. For each image frame of size $(H = 96, W = 96, C = 3)$, the VQ-VAE-visual encoder compresses it into a discrete latent representation of size $(H' = 24, W' = 24)$. The VQ-VAE-audio and the VQ-VAE-visual codebooks contain, respectively, $k_a = 256$ and $k_v = 512$ codes of dimension $e_a = 8$ and $e_v = 4$. Such a low dimension is chosen to increase the use of the different codes in the codebook (Yu et al., 2021).

VQ-MAE-AV architectures. The VQ-MAE-AV model uses $L = 12$ attention blocks in the encoder and $L' = 4$ in the decoder. Each self-attention layer of a block is divided

into *four* heads. By default, the parameters of the discrete audio and visual tokens (d , h , and w) are set to 4. We set $t_a = 10$ and $t_v = 5$ because the sampling rate of $\mathbf{x}^{(a)}$ is twice the sampling rate of $\mathbf{x}^{(v)}$. In the ablation study (Section 4.4), we will explore all possible combinations of the VQ-MAE-AV encoder and decoder, according to the two fusion strategies (*self-attention fusion* and *cross-attention fusion*). We will also evaluate the impact of the pooling strategy and contrastive learning.

4.1.3. Training and fine-tuning details

Self-supervised training details. The VQ-MAE-AV is trained using the AdamW optimizer (Loshchilov & Hutter, 2017) with a cosine scheduler to adjust the learning rate, with a 100-epoch warm-up period. The parameters of the optimizer, similar to He et al. (2022), are $\beta_1 = 0.9$, $\beta_2 = 0.95$, and $\text{weight_decay} = 0.05$. The base learning rate follows the linear scaling rule (Goyal et al., 2017) $lr = (\text{base_lr} = 1e - 3) \times (\text{batchsize} = 128) / 256$. We distributed the pre-training of VQ-MAE-AV on 4 NVIDIA HGX A100. The training lasted for 160 epochs, and each epoch took approximately 15 minutes.

Table 1: Accuracy (%) and F1 score (%) results of audiovisual SER. VQ-MAE-AV is pre-trained with both the generative (3) and contrastive (4) loss functions using the Query2Emo pooling strategy. The best scores are in bold, and the second-best scores are underlined.

RAVDESS			CREMA-D		
Method	Accuracy	F1 score	Method	Accuracy	F1 score
AV-LSTM (Ghaleb et al., 2019)	65.80	-	AV-LSTM (Ghaleb et al., 2019)	72.90	-
MuLT (Tsai et al., 2019)	76.60	77.30	MATER (Ghaleb et al., 2020)	67.20	-
CFN-SR (Fu et al., 2021)	75.76	-	RAVER (Goncalves & Busso, 2022)	<u>77.30</u>	-
MATER (Ghaleb et al., 2020)	76.30	-	MuT Base (Tran & Soleymani, 2022)	68.87	-
AVT (Chumachenko et al., 2022)	79.20	78.20	MuT Large (Tran & Soleymani, 2022)	70.22	-
MDVAE (Sadok et al., 2024)	<u>79.30</u>	<u>80.70</u>	AV-Gating (Ghaleb et al., 2019)	74.00	-
VQ-MAE-AV (ours)	84.80	84.50	VQ-MAE-AV (ours)	80.40	80.00

Fine-tuning details. For the fine-tuning process, we also use the AdamW optimizer (Loshchilov & Hutter, 2017) with a cosine scheduler to adjust the learning rate and with a 40-epoch warm-up period. The parameters of the optimizer are the same as those used for the pre-training. The base learning rate is $1e-4$.

4.2. Audiovisual speech reconstruction quality

In this experiment, we evaluate the reconstruction quality of VQ-MAE-AV when applied to masked audiovisual speech data. The model is fed with a sequence of tokens, some of which have been masked, and it is used to predict the masked tokens, i.e. to reconstruct the complete audiovisual speech sequence from partially observed tokens. We will study the reconstruction performance for different masking ratios.

For this experiment, we compare VQ-MAE-AV to VQ-MAE-A (A for audio) and VQ-MAE-V (V for visual), which are the unimodal versions of VQ-MAE-AV. The average quality performance for the speech and visual modalities is evaluated using the VoxCeleb2 test set. The Peak Signal-to-Noise Ratio (PSNR in dB) is used to assess the quality of the resynthesized visual data, and the Signal-to-Distortion Ratio (SDR in dB) is used to assess the quality of the resynthesized audio data.

Fig. 4a and Fig.4b present the PSNR and SDR curves, respectively, for the reconstruction quality of the visual and audio modalities as a function of the masking ratio. Notably, VQ-MAE-AV outperforms VQ-MAE-V for masking ratios greater than 50%. At a masking ratio of 90%, VQ-MAE-AV achieves a significant 3.68 dB gain in PSNR over VQ-MAE-V. For the audio modality, VQ-MAE-AV outperforms VQ-MAE-A for masking ratios greater than 40% and records a gain of 2.87 dB in SDR at 90% of masking. In summary, this experiment highlights the effectiveness of leveraging multimodality to improve reconstruction quality.

4.3. Audiovisual emotion recognition

Table 1 compares the emotion recognition performance (accuracy and F1 score) of the proposed VQ-MAE-AV model (using the *cross-attention fusion* strategy for both the encoder and decoder) with the performance of several audiovisual state-of-the-art methods.

The experimental comparison includes LSTM-based methods (Ghaleb et al., 2019) and Transformer-based methods (Tsai et al., 2019; Chumachenko et al., 2022; Goncalves & Busso, 2022). MATER (Ghaleb et al., 2020) uses distinct Transformer architectures for each modality, merging the embeddings via mean pooling. CFN-SR (Fu et al., 2021) introduces a cross-modality learning approach, employing self-attention and residual structures to model inter- and intra-modality interactions. We also consider the AVT method (Chumachenko et al., 2022), which uses self-attention fusion and modality dropout to address the challenge of one modality being absent. Additionally, RAVER (Goncalves & Busso, 2022) addresses challenges related to modality alignment, temporal information capture, and handling missing features.

The experimental comparison also includes unsupervised audiovisual approaches, such as the multimodal dynamical VAE (MDVAE) (Sadok et al., 2024), which employs a hierarchical latent space to segregate static from dynamic information and modality-common from modality-specific information. Additionally, we compare with MuT (Tran & Soleymani, 2022), a self-supervised approach using the Transformer architecture and pre-trained on the VoxCeleb dataset with a pretext task of reconstructing masked frames (with a masking ratio of 15%).

As can be seen in Table 1, the VQ-MAE-AV model with Query2Emo outperforms the most recent methods overall. VQ-MAE-AV achieves 9.04%, 5.60% and 5.50% better accuracy than the CFN-SR (Fu et al., 2021), AVT (Chumachenko et al., 2022) and MDVAE (Sadok et al., 2024) methods for the RAVDESS dataset, respectively. Regarding the CREMA-D dataset, VQ-MAE-AV achieves 7.50%, 6.40%, and 3.10% better accuracy than the AV-

Table 2: Performance of VQ-MAE-AV using the *self-attention fusion* strategy for both encoder and decoder, and using the attention pooling strategy for the fine-tuning. ‘Pre-train’ refers to the training of the VQ-MAE-AV for the unmasking task on the VoxCeleb2 database. ‘Freeze’ refers to the freezing of the VQ-MAE-AV encoder.

Method	Pre-train	Freeze	Accuracy (%)
VQ-MAE-AV	✗	✗	29.6
VQ-MAE-AV	✓	✓	70.5
VQ-MAE-AV	✓	✗	81.5

Table 4: Performance of VQ-MAE-AV using the *self-attention fusion* strategy for both encoder and decoder, and using the Query2Emo pooling strategy for the fine-tuning. ‘Generative’ corresponds to the loss function in Eq. 3 and ‘Contrastive’ corresponds to the loss function in Eq. 4.

Method	Contrastive	Generative	Accuracy (%)
VQ-MAE-AV	✓	✗	75.2
VQ-MAE-AV	✗	✓	84.3
VQ-MAE-AV	✓	✓	84.8

Table 6: Performance of VQ-MAE-AV using the *self-attention fusion* strategy for both encoder and decoder, without contrastive learning, and using different pooling strategies for the fine-tuning.

Pooling strategy	Accuracy (%)	F1 score (%)
Mean Pooling	78.1	78.4
Attention Pooling	81.5	80.1
Query2Emo	84.3	84.8

LSTM (Ghaleb et al., 2019), AV-Gating (Ghaleb et al., 2019), and RAVER (Goncalves & Busso, 2022). Overall, the experimental results demonstrate the effectiveness of the proposed audiovisual self-supervised representation learning technique for SER. This indicates that VQ-MAE-AV learns audiovisual representations that are effectively transferable to the emotion recognition task, resulting in improved performance compared to audiovisual state-of-the-art methods.

4.4. Ablation study and model properties

We conduct a series of experiments to evaluate the impact of various hyperparameters and model designs on the emotion recognition performance of the proposed VQ-MAE-AV model. In the following paragraphs, we will present and discuss the findings of these experiments. All the ablation study is done on RAVDESS.

4.4.1. Impact of pre-training and fine-tuning

Table 2 shows the significance of pre-training and fine-tuning the VQ-MAE-AV model for audiovisual SER. Pre-training the model for the unmasking task on the VoxCeleb2 database substantially improves the emotion recognition performance, with the accuracy rising from 29.6% to 81.5%. Fine-tuning the encoder is also essential, as keeping it frozen leads to a 11% drop in accuracy.

Table 3: Performance of VQ-MAE-AV using the *self-attention fusion* strategy for both encoder and decoder, fine-tuned on RAVDESS for different encoder depths.

Method	Param. (M)	Acc. (%)	F1 score (%)
VQ-MAE-AV-6	8.5	75.7	76.0
VQ-MAE-AV-12	13.5	81.5	80.1
VQ-MAE-AV-16	16.8	82.4	82.4
VQ-MAE-AV-20	20.2	81.3	81.3

Table 5: Performance of VQ-MAE-AV without contrastive learning for different encoder and decoder architectures, using the attention pooling strategy for the fine-tuning. *SAF* stands for *self-attention fusion* and *CAF* stands for *cross-attention fusion*.

Method	Param. (M)	Encoder	Decoder	Acc. (%)
VQ-MAE-AV	13.5	<i>SAF</i>	<i>SAF</i>	81.5
VQ-MAE-AV	25.0	<i>CAF</i>	<i>SAF</i>	82.8
VQ-MAE-AV	18.4	<i>SAF</i>	<i>CAF</i>	81.8
VQ-MAE-AV	30.0	<i>CAF</i>	<i>CAF</i>	83.0

Table 7: Comparison of performance between unimodal VQ-MAE-A-12 or VQ-MAE-V-12 and multimodal VQ-MAE-AV-12 (using SAF for both encoder and decoder and without contrastive learning).

Method	Accuracy (%)	F1 score (%)
VQ-MAE-A-12	73.2	72.8
VQ-MAE-V-12	74.1	73.9
VQ-MAE-AV-12	81.5	80.1

4.4.2. Impact of the encoder depth

Table 3 shows the impact of encoder depth on emotion recognition performance by varying the number of attention blocks (L), where a model with n attention blocks in the encoder will be denoted by VQ-MAE-AV- n . The results show that increasing the number of blocks in the encoder leads to improved performance to a certain extent. However, when the number of blocks becomes too high (as in the case of VQ-MAE-AV-20), there is no further improvement, and performance actually decreases by 1.1% accuracy compared to VQ-MAE-AV-16.

4.4.3. Impact of the contrastive learning

The influence of contrastive learning on emotion recognition is illustrated in Table 4. When training VQ-MAE-AV exclusively with the contrastive loss, the achieved accuracy is 75.2%, which is 9.1% lower than when using only the generative loss. Notably, the combination of both losses, contrastive and generative, leads to improved emotion recognition, resulting in a 0.5% accuracy boost compared to using the generative loss alone.

4.4.4. Impact of the encoder/decoder architecture

Table 5 shows the performance of the four different configurations of the VQ-MAE-AV model described in Section 3.5, including all possible combinations of the fusion strategies for the VQ-MAE-AV encoder and decoder: *self-attention fusion* for both the encoder and de-

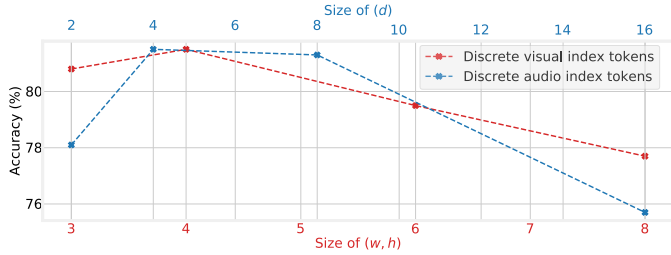


Figure 5: Impact of the discrete audio and visual token size on emotion recognition.

coder (SAF-SAF); *self-attention fusion* for the encoder and *cross-attention fusion* for the decoder (SAF-CAF); *cross-attention fusion* for the encoder and *self-attention fusion* for the decoder (CAF-SAF); and *cross-attention fusion* for both the encoder and decoder (CAF-CAF). Among these configurations, CAF-CAF achieves the highest accuracy with a 1.5% improvement over SAF-SAF, followed by CAF-SAF with a 1.3% improvement over SAF-SAF, and then SAF-CAF with only a 0.3% improvement. The *cross-attention fusion* encoder architecture achieves the best performance in emotion recognition, as shown by the CAF-CAF and CAF-SAF configurations. However, there exists a trade-off between performance and the number of model parameters. Notably, CAF-CAF involves slightly more than twice as many parameters as SAF-SAF.

4.4.5. Impact of the pooling strategy

Table 6 presents the impact of various pooling strategies when fine-tuning the model for audiovisual SER. The results reveal that attention-based pooling techniques, such as attention pooling and Query2Emo, outperform mean pooling. Among the two attention-based methods, Query2Emo outperforms attention pooling, with an accuracy gain of 2.8%.

4.4.6. Impact of the audio and visual discrete token size

Fig. 5 shows the impact of the dimensions of the discrete tokens for the visual (h and w) and audio (d) modalities on the audiovisual SER performance. The values of h and w represent the visual token size on the horizontal and vertical axes, respectively, while d represents the token size on the frequency axis of the audio modality. Our study reveals that the performance of emotion recognition is impacted by both (h, w) and d values. Therefore, it is important to select these parameters carefully. Based on our experiments, we recommend fixing them to ($h = w = 4, d = 4$).

4.4.7. Impact of the audiovisual inputs

Table 7 compares our approach VQ-MAE-AV with its unimodal versions (VQ-MAE-V and VQ-MAE-A). The VQ-MAE-AV model exhibits improved performance over VQ-MAE-V and VQ-MAE-A, with gains of 5.6% and 8.3% in accuracy, respectively. This indicates the effectiveness of incorporating audiovisual information in the self-supervised

paradigm, leading to better performance in emotion recognition.

5. Conclusion

Masked autoencoder modeling is a versatile self-supervised learning approach that can be adapted to various types of data. This paper introduced the VQ-MAE-AV model for learning representations of audiovisual speech data, which could be extended to other multimodal sequential data. VQ-MAE-AV took as input a discrete audio representation and a discrete visual representation obtained via two separate VQ-VAEs. These representations were then divided into multiple discrete tokens, with spatio-temporal tokens for the visual modality and spectro-temporal tokens for the audio modality. Pre-trained on the VoxCeleb2 dataset and fine-tuned on standard emotional audiovisual speech datasets, the experiments showed that the VQ-MAE-AV model effectively combined the audio and visual modalities for audiovisual SER, outperforming several state-of-the-art methods.

For future work, we plan to investigate other masking strategies and increase the resolution of the images to further improve emotion recognition performance. We could also explore using the representation learned by the proposed VQ-MAE-AV model for other downstream tasks in audiovisual speech processing, such as speaker recognition.

Acknowledgments

This work was performed using computational resources from the “Mésocentre” computing center of Université Paris-Saclay, CentraleSupélec and École Normale Supérieure Paris-Saclay supported by CNRS and Région Île-de-France (<https://mesocentre.universite-paris-saclay.fr/>)

References

- Akbari, H., Yuan, L., Qian, R., Chuang, W.-H., Chang, S.-F., Cui, Y., & Gong, B. (2021). VATT: Transformers for multimodal self-supervised learning from raw video, audio and text. *Advances in Neural Information Processing Systems (NeurIPS)*, 34, 24206–24221.
- Alayrac, J.-B., Recasens, A., Schneider, R., Arandjelović, R., Ramapuram, J., De Fauw, J., Smaira, L., Dieleman, S., & Zisserman, A. (2020). Self-supervised multimodal versatile networks. *Advances in Neural Information Processing Systems (NeurIPS)*, 33, 25–37.
- Arnab, A., Dehghani, M., Heigold, G., Sun, C., Lučić, M., & Schmid, C. (2021). ViViT: A video vision transformer. In *IEEE/CVF International Conference on Computer Vision (ICCV)* (pp. 6836–6846).
- Arnela, M., Blandin, R., Dabbaghchian, S., Guasch, O., Alías, F., Pelorson, X., Van Hirtum, A., & Engwall, O. (2016). Influence of lips on the production of vowels based on finite element simulations and experiments. *The Journal of the Acoustical Society of America*, 139, 2852–2859.
- Baade, A., Peng, P., & Harwath, D. (2022). MAE-AST: Masked autoencoding audio spectrogram transformer. In *International Speech Communication Association (Interspeech)* (pp. 2438–2442).

- Bachmann, R., Mizrahi, D., Atanov, A., & Zamir, A. (2022). Multi-MAE: Multi-modal multi-task masked autoencoders. In *European Conference on Computer Vision (ECCV)* (pp. 348–367). Springer.
- Bao, H., Dong, L., Piao, S., & Wei, F. (2021). BEiT: BERT pre-training of image transformers. In *International Conference on Learning Representations (ICLR)*.
- Bengio, Y., Lamblin, P., Popovici, D., & Larochelle, H. (2006). Greedy layer-wise training of deep networks. *Advances in Neural Information Processing Systems (NeurIPS)*, 19.
- Bulat, A., & Tzimiropoulos, G. (2017). How far are we from solving the 2D & 3D Face Alignment problem? (and a dataset of 230,000 3D facial landmarks). In *IEEE/CVF International Conference on Computer Vision (ICCV)*.
- Busso, C., Bulut, M., Lee, C.-C., Kazemzadeh, A., Mower, E., Kim, S., Chang, J. N., Lee, S., & Narayanan, S. S. (2008). IEMOCAP: Interactive emotional dyadic motion capture database. *Language resources and evaluation*, 42, 335–359.
- Cao, H., Cooper, D. G., Keutmann, M. K., Gur, R. C., Nenkova, A., & Verma, R. (2014). CREMA-D: Crowd-sourced emotional multimodal actors dataset. *IEEE Transactions on Affective Computing*, 5, 377–390.
- Chen, L.-W., & Rudnick, A. (2023). Exploring wav2vec 2.0 fine tuning for improved speech emotion recognition. In *IEEE International Conference on Acoustics, Speech and Signal Processing (ICASSP)* (pp. 1–5). IEEE.
- Chen, T., Kornblith, S., Norouzi, M., & Hinton, G. (2020a). A simple framework for contrastive learning of visual representations. In *International Conference on Machine Learning (ICML)* (pp. 1597–1607). PMLR.
- Chen, X., Fan, H., Girshick, R., & He, K. (2020b). Improved baselines with momentum contrastive learning. *arXiv preprint arXiv:2003.04297*, .
- Chumachenko, K., Iosifidis, A., & Gabbouj, M. (2022). Self-attention fusion for audiovisual emotion recognition with incomplete data. In *International Conference on Pattern Recognition (ICPR)* (pp. 2822–2828). IEEE.
- Chung, J., Nagrani, A., & Zisserman, A. (2018). VoxCeleb2: Deep speaker recognition. In *International Speech Communication Association (Interspeech)* (pp. 1086–1090). doi:10.21437/Interspeech.2018-1929.
- Devlin, J., Chang, M.-W., Lee, K., & Toutanova, K. (2019). BERT: Pre-training of deep bidirectional transformers for language understanding. *Conference of the North American Chapter of the Association for Computational Linguistics: Human Language Technologies, Volume 1 (Long and Short Papers)*, (pp. 4171–4186).
- Dib, A., Ahn, J., Thebault, C., Gosselin, P.-H., & Chevallier, L. (2023). S2f2: Self-supervised high fidelity face reconstruction from monocular image. In *IEEE International Conference on Automatic Face and Gesture Recognition (FG)* (pp. 1–8). IEEE.
- Dong, X., Bao, J., Zhang, T., Chen, D., Zhang, W., Yuan, L., Chen, D., Wen, F., & Yu, N. (2021). PeCo: Perceptual codebook for BERT pre-training of vision transformers. *arXiv preprint arXiv:2111.12710*, .
- Dosovitskiy, A., Beyer, L., Kolesnikov, A., Weissenborn, D., Zhai, X., Unterthiner, T., Dehghani, M., Minderer, M., Heigold, G., Gelly, S. et al. (2020). An image is worth 16x16 words: Transformers for image recognition at scale. *International Conference on Learning Representations (ICLR)*, .
- El Ayadi, M., Kamel, M. S., & Karray, F. (2011). Survey on speech emotion recognition: Features, classification schemes, and databases. *Pattern recognition*, 44, 572–587.
- Esser, P., Rombach, R., & Ommer, B. (2021). Taming transformers for high-resolution image synthesis. In *IEEE/CVF conference on computer vision and pattern recognition (CVPR)* (pp. 12873–12883).
- Feichtenhofer, C., Li, Y., He, K. et al. (2022). Masked autoencoders as spatiotemporal learners. *Advances in Neural Information Processing Systems (NeurIPS)*, 35, 35946–35958.
- Févotte, C., Bertin, N., & Durrieu, J.-L. (2009). Nonnegative matrix factorization with the Itakura-Saito divergence: With application to music analysis. *Neural computation*, 21, 793–830.
- Fu, Z., Liu, F., Wang, H., Qi, J., Fu, X., Zhou, A., & Li, Z. (2021). A cross-modal fusion network based on self-attention and residual structure for multimodal emotion recognition. *arXiv preprint arXiv:2111.02172*, .
- Gan, C., Huang, D., Zhao, H., Tenenbaum, J. B., & Torralba, A. (2020). Music gesture for visual sound separation. In *IEEE/CVF Conference on Computer Vision and Pattern Recognition (CVPR)* (pp. 10478–10487).
- Gao, R., & Grauman, K. (2019). Co-separating sounds of visual objects. In *IEEE/CVF International Conference on Computer Vision (ICCV)* (pp. 3879–3888).
- Geng, X., Liu, H., Lee, L., Schuurams, D., Levine, S., & Abbeel, P. (2022). Multimodal masked autoencoders learn transferable representations. *arXiv preprint arXiv:2205.14204*, .
- Ghaleb, E., Niehues, J., & Asteriadis, S. (2020). Multimodal attention-mechanism for temporal emotion recognition. In *IEEE International Conference on Image Processing (ICIP)* (pp. 251–255). IEEE.
- Ghaleb, E., Popa, M., & Asteriadis, S. (2019). Multimodal and temporal perception of audio-visual cues for emotion recognition. In *International Conference on Affective Computing and Intelligent Interaction (ACII)* (pp. 552–558). IEEE.
- Gidaris, S., Singh, P., & Komodakis, N. (2018). Unsupervised representation learning by predicting image rotations. In *International Conference on Learning Representations (ICLR)*.
- Goncalves, L., & Busso, C. (2022). Robust audiovisual emotion recognition: Aligning modalities, capturing temporal information, and handling missing features. *IEEE Transactions on Affective Computing*, 13, 2156–2170.
- Gong, Y., Lai, C.-I., Chung, Y.-A., & Glass, J. (2022a). SSAST: Self-supervised audio spectrogram transformer. In *AAAI Conference on Artificial Intelligence* (pp. 10699–10709). volume 36.
- Gong, Y., Rouditchenko, A., Liu, A. H., Harwath, D., Karlinsky, L., Kuehne, H., & Glass, J. R. (2022b). Contrastive audio-visual masked autoencoder. In *International Conference on Learning Representations (ICLR)*.
- Goyal, P., Dollár, P., Girshick, R., Noordhuis, P., Wesolowski, L., Kyrola, A., Tulloch, A., Jia, Y., & He, K. (2017). Accurate, large minibatch SGD: Training imagenet in 1 hour. *arXiv preprint arXiv:1706.02677*, .
- He, K., Chen, X., Xie, S., Li, Y., Dollár, P., & Girshick, R. (2022). Masked autoencoders are scalable vision learners. In *IEEE/CVF Conference on Computer Vision and Pattern Recognition (CVPR)* (pp. 16000–16009).
- Huang, P.-Y., Xu, H., Li, J., Baevski, A., Auli, M., Galuba, W., Metzger, F., & Feichtenhofer, C. (2022). Masked autoencoders that listen. *Advances in Neural Information Processing Systems (NeurIPS)*, 35, 28708–28720.
- Huang, Z., Jin, X., Lu, C., Hou, Q., Cheng, M.-M., Fu, D., Shen, X., & Feng, J. (2023). Contrastive masked autoencoders are stronger vision learners. *IEEE Transactions on Pattern Analysis and Machine Intelligence*, 46, 1–13.
- Jegorova, M., Petridis, S., & Pantic, M. (2023). SS-VAERR: Self-supervised apparent emotional reaction recognition from video. In *IEEE International Conference on Automatic Face and Gesture Recognition (FG)* (pp. 1–8). IEEE.
- Li, T., Chang, H., Mishra, S., Zhang, H., Katabi, D., & Krishnan, D. (2023). MAGE: Masked generative encoder to unify representation learning and image synthesis. In *IEEE/CVF Conference on Computer Vision and Pattern Recognition (CVPR)* (pp. 2142–2152).
- Liu, S., Mallol-Ragolta, A., Parada-Cabaleiro, E., Qian, K., Jing, X., Kathan, A., Hu, B., & Schuller, B. W. (2022). Audio self-supervised learning: A survey. *Patterns*, 3, 100616.
- Liu, S., Zhang, L., Yang, X., Su, H., & Zhu, J. (2021). Query2label: A simple transformer way to multi-label classification. *preprint arXiv:2107.10834*, .
- Livingstone, S. R., & Russo, F. A. (2018). The Ryerson audio-visual database of emotional speech and song (RAVDESS): A dynamic, multimodal set of facial and vocal expressions in north american english. *PLoS one*, 13.
- Loshchilov, I., & Hutter, F. (2017). Decoupled weight decay regu-

- larization. *International Conference on Learning Representations (ICLR)*, .
- Mehrabian, A. (2017). *Nonverbal communication*. Routledge.
- Noroozi, M., & Favaro, P. (2016). Unsupervised learning of visual representations by solving jigsaw puzzles. In *Computer Vision (ECCV)* (pp. 69–84). Springer.
- Pepino, L., Riera, P., & Ferrer, L. (2021). Emotion recognition from speech using wav2vec 2.0 embeddings. *International Speech Communication Association (Interspeech)*, (pp. 3400–3404).
- Ramachandram, D., & Taylor, G. W. (2017). Deep multimodal learning: A survey on recent advances and trends. *IEEE Signal Processing Magazine*, *34*, 96–108.
- Ridnik, T., Ben-Baruch, E., Zamir, N., Noy, A., Friedman, I., Protter, M., & Zelnik-Manor, L. (2021). Asymmetric loss for multi-label classification. In *IEEE/CVF International Conference on Computer Vision (ICCV)* (pp. 82–91). IEEE Computer Society.
- Sadok, S., Leglaive, S., Girin, L., Alameda-Pineda, X., & Séguier, R. (2024). A multimodal dynamical variational autoencoder for audiovisual speech representation learning. *Neural Networks*, *172*, 106120. URL: <https://www.sciencedirect.com/science/article/pii/S0893608024000340>.
- Sadok, S., Leglaive, S., & Séguier, R. (2023). A vector quantized masked autoencoder for speech emotion recognition. In *IEEE ICASSP 2023 Workshop on Self-Supervision in Audio, Speech and Beyond (SASB)*.
- Schoneveld, L., Othmani, A., & Abdelkawy, H. (2021). Leveraging recent advances in deep learning for audio-visual emotion recognition. *Pattern Recognition Letters*, *146*, 1–7.
- Tong, Z., Song, Y., Wang, J., & Wang, L. (2022). Videomae: Masked autoencoders are data-efficient learners for self-supervised video pre-training. *Advances in Neural Information Processing Systems (NeurIPS)*, *35*, 10078–10093.
- Touvron, H., Cord, M., El-Nouby, A., Bojanowski, P., Joulin, A., Synnaeve, G., & Jégou, H. (2021). Augmenting convolutional networks with attention-based aggregation. *arXiv preprint arXiv:2112.13692*, .
- Tran, M., & Soleymani, M. (2022). A pre-trained audio-visual transformer for emotion recognition. In *IEEE International Conference on Acoustics, Speech and Signal Processing (ICASSP)* (pp. 4698–4702). IEEE.
- Tsai, Y.-H. H., Bai, S., Liang, P. P., Kolter, J. Z., Morency, L.-P., & Salakhutdinov, R. (2019). Multimodal transformer for unaligned multimodal language sequences. In *Association for Computational Linguistics. Meeting* (p. 6558). NIH Public Access volume 2019.
- Van Den Oord, A., Vinyals, O. et al. (2017). Neural discrete representation learning. *Advances in Neural Information Processing Systems (NeurIPS)*, *30*.
- Vaswani, A., Shazeer, N., Parmar, N., Uszkoreit, J., Jones, L., Gomez, A. N., Kaiser, L., & Polosukhin, I. (2017). Attention is all you need. *Advances in Neural Information Processing Systems (NeurIPS)*, *30*.
- Wang, Y., Boumadane, A., & Heba, A. (2021). A fine-tuned wav2vec 2.0/hubert benchmark for speech emotion recognition, speaker verification and spoken language understanding. *arXiv preprint arXiv:2111.02735*, .
- Xie, Z., Zhang, Z., Cao, Y., Lin, Y., Bao, J., Yao, Z., Dai, Q., & Hu, H. (2022). Simmim: A simple framework for masked image modeling. In *IEEE/CVF Conference on Computer Vision and Pattern Recognition (CVPR)* (pp. 9653–9663).
- Yu, J., Li, X., Koh, J. Y., Zhang, H., Pang, R., Qin, J., Ku, A., Xu, Y., Baldrige, J., & Wu, Y. (2021). Vector-quantized image modeling with improved vqgan. In *International Conference on Learning Representations (ICLR)*.
- Zhang, C., Zhang, C., Song, J., Yi, J. S. K., Zhang, K., & Kweon, I. S. (2022). A survey on masked autoencoder for self-supervised learning in vision and beyond. *arXiv preprint arXiv:2208.00173*, .
- Zhao, H., Gan, C., Ma, W.-C., & Torralba, A. (2019). The sound of motions. In *IEEE/CVF International Conference on Computer Vision (ICCV)* (pp. 1735–1744).